The Journal of Immunology

αPIX RhoGEF Supports Positive Selection by Restraining Migration and Promoting Arrest of Thymocytes

Mark Korthals, Kerstin Schilling, Peter Reichardt, Dejan Mamula, Thomas Schlüter, Michael Steiner, Kristina Langnäse, Ulrich Thomas, Eckart Gundelfinger, Richard T. Premont, Kerry Tedford and Klaus-Dieter Fischer

J Immunol 2014; 192:3228-3238; Prepublished online 3 March 2014;
doi: 10.4049/jimmunol.1302585
http://www.jimmunol.org/content/192/7/3228

The Journal of Immunology is published twice each month by
The American Association of Immunologists, Inc.,
1451 Rockville Pike, Suite 650, Rockville, MD 20852

Print ISSN: 0022-1767 Online ISSN: 1550-6606.

αPIX RhoGEF Supports Positive Selection by Restraining Migration and Promoting Arrest of Thymocytes

Mark Korthals,*[,1] Kerstin Schilling,*[,1] Peter Reichardt,[†] Dejan Mamula,[‡] Thomas Schlüter,[‡] Michael Steiner,[‡] Kristina Langnäse,[‡] Ulrich Thomas,[§] Eckart Gundelfinger,[§] Richard T. Premont,[¶] Kerry Tedford,* and Klaus-Dieter Fischer*[,‡]

Thymocytes mature in a series of stages by migrating through specific areas of the thymus and interacting with other cells to receive the necessary developmental signals; however, little is known about the molecular mechanisms governing this migration. We report that murine thymocytes with a knockout mutation in α-PAK (p21-activated kinase)-interacting exchange factor (PIX; Arhgef6), an activator of Rho GTPases, showed greatly increased motility and altered morphology in two-dimensional migration on ICAM-1. αPIX was also required for efficient positive selection, but not negative selection, of thymocytes. TCR signaling was normal in *αPix*$^{-}$ thymocytes, indicating that the effects of αPIX on positive selection are largely independent of TCR signaling. *αPix*$^{-}$ thymocytes also paused less during migration in the thymic cortex, interacted less with ICAM-1 coated beads, and could overcome TCR stop signals, consistent with defective scanning behavior. These results identify αPIX as a regulator of thymocyte migration and subsequent arrest that is linked to positive selection. ***The Journal of Immunology*****, 2014, 192: 3228–3238.**

Thymocyte maturation is a dynamic process that occurs in distinct spatial compartments of the thymus with the ultimate goal of producing a T cell bearing a functional and non–self-reactive TCR (1, 2). The earliest thymocyte progenitors, known as double-negative (DN) thymocytes, rearrange TCR and upregulate CD4 and CD8 coreceptors to yield $CD4^{+}$ $CD8^{+}$ double-positive (DP) thymocytes. A fraction of DP thymocytes successfully receive TCR-activating signals from APCs, such as cortical thymic epithelial cells (cTEC), macrophages, or dendritic cells (DCs), carrying self-peptide in a complex with MHC (pMHC). These cells are then selected for positive selection while the rest of the DP thymocytes die of TCR neglect. Positively selected DP thymocytes then become $CD4^{+}$ or $CD8^{+}$ single-positive (SP) thymocytes and migrate to the medulla, where autoreactive thymocytes are eliminated by negative selection.

Various two-photon imaging studies have shown that thymocyte motility is affected by the process of positive selection (3–5), but the molecular mechanisms regulating this migration are unclear. An analysis of thymocytes from mice with a mutation in *Git2* (G protein–coupled receptor kinase interacting ArfGAP 2), an ArfGAP involved in vesicle transport and receptor recycling, revealed a block in development at the DP stage (6). *Git2*$^{-/-}$ thymocytes migrate faster than wild type in vitro; however, two-photon microscopy in the thymus showed that *Git2*$^{-/-}$ thymocytes are significantly less motile in vivo. They accumulate near blood vessels in the cortex, leading to the suggestion that they are immobilized by a hyperreactive chemokine response (6). In the medulla, thymocyte migration is impaired by blocking LFA-1 integrin or by deleting its ligand ICAM-1 (7). Additional factors known to influence localization of thymocytes to the cortex or medulla include chemokines, substrate, and contact with stromal cell "highways" (8, 9).

The PAK (p21-activated kinase)-interacting exchange factor (PIX) proteins, αPIX and βPIX, are multidomain Rho GTPase guanine nucleotide exchange factors (RhoGEFs) that can activate Rac and Cdc42 GTPases. PIX proteins bind constitutively to GIT2 and its homolog GIT1, and together the four proteins form a large oligomeric complex (10, 11). Thus, PIX proteins relay signals from receptors through GTPases to the actin cytoskeleton and act as scaffold proteins for additional signaling intermediates. We previously reported that *αPix*$^{-}$ mice have reduced numbers of peripheral T and B cells, and *αPix*$^{-}$ T cells show greatly increased rates of basal and CXCL12-induced migration (12). Although αPIX and βPIX have both been implicated in cytoskeletal dynamics such as migration, focal adhesion, and polarization in other cell types (12–15), the role of PIX proteins in thymocyte development and functions is unknown.

To define a role for αPIX in thymocytes, we analyzed thymocyte development and motility in *αPix*$^{-}$ mice. We report that αPIX was required for efficient positive selection of TCR-transgenic DP thymocytes, but not for H-Y–induced negative selection. *αPix*$^{-}$ thymocytes showed greatly increased migration in transwell and two-dimensional (2D) migration assays. The pronounced increase in migration was confirmed in vivo using two-photon microscopy of the thymic cortex. The deregulation of *αPix*$^{-}$ thymocyte migration was strong enough to override TCR

*Department of Functional Genomics and Medical Toponomics, Otto-von-Guericke-University, Medical Faculty, Magdeburg 39120, Germany; [†]Institute of Molecular and Clinical Immunology, Otto-von-Guericke-University, Medical Faculty, Magdeburg 39120, Germany; [‡]Institute of Biochemistry and Cell Biology, Otto-von-Guericke-University, Medical Faculty, Magdeburg 39120, Germany; [§]Leibniz Institute for Neurobiology, Magdeburg 39120, Germany; and [¶]Department of Medicine, Duke University Medical Center, Durham, NC 27701

[1]M.K. and K.S. contributed equally to this work.

Received for publication September 26, 2013. Accepted for publication February 3, 2014.

This work was supported by a grant from Deutsche Forschungsgemeinschaft (SFB 854 to U.T., E.G., and K.-D.F.).

Address correspondence and reprint requests to Dr. Klaus-Dieter Fischer, Institute of Biochemistry and Cell Biology, Otto-von-Guericke-University, Medical Faculty, Leipziger Straße 44, 39120 Magdeburg, Germany. E-mail address: klaus.fischer@med.ovgu.de.

The online version of this article contains supplemental material.

Abbreviations used in this article: 7-AAD, 7-aminoactinomycin D; cTEC, cortical thymic epithelial cell; 2D, two dimensional; DC, dendritic cell; DN, double negative; DP, double positive; GPCR, G protein-coupled receptor; PIX, PAK (p21-activated kinase)–interacting exchange factor; pMHC, peptide-bound MHC; RhoGEF, Rho GTPase guanine nucleotide exchange factor; SP, single positive.

www.jimmunol.org/cgi/doi/10.4049/jimmunol.1302585

stop signals and ICAM-1–mediated contacts, although general TCR-induced signaling was normal, highlighting a probable role for αPIX in thymocyte scanning of cTECs. These results show that αPIX restrains migration and consequently promotes arrest, and that both functions correlate with efficient positive selection.

Materials and Methods

Mice and cell lines

αPix^{-} mice (12) were backcrossed on the BALB/C (Charles River) or C57BL/6J (Charles River) background for more than 10 generations and then intercrossed with DO11.10^{+} (16), OT-II^{+} (17), and H-Y^{+} (18) mice. Eight- to twelve-week-old littermates or age-matched mice were analyzed. For two-photon analysis, *αPix*$^{-}$ mice (C57BL/6) were crossed to histone-GFP mice (19) and rosa26 tdRFP mice (20). Expression of RFP was induced by pTα−Cre (20). *Git2*$^{-/-}$ mice (21) on a C57BL/6 background were crossed to OT-II^{+} mice, and heterozygous offspring were analyzed. OP9-DL1 cells have been described previously (22). Reconstituted mice were generated by transferring 2×10^6 bone marrow cells from TCR transgenic DO11.10^{+} wild type or *αPix*$^{-}$ BALB/C mice to lethally irradiated (1000 rad) hosts. Animals were housed in specific pathogen–free conditions according to institutional guidelines.

In vitro cell migration

Cell migration on 2D surfaces was analyzed by coating the wells of a μ-Slide (Ibidi, Martinsried, Germany) with 10 μg/ml recombinant mouse ICAM-1/human Fc chimera (R&D Systems, Abingdon, U.K.) or 2 μg/ml CXCL12 (R&D Systems), or both, as indicated and blocked with 2% BSA. Thymocytes were stained with 0.2 μM CFDA-SE or 2 μM orange CMRA (Life Technologies) and resuspended in buffer containing 1 mM Ca^{2+} and Mg^{2+}. Soluble CXCL12 was added at 200 ng/ml where indicated. For migration on stromal cells, thymocytes were stained as above and seeded on OP9-DL1 cell monolayers. For analysis of thymocytes interacting with ICAM-1–coated beads, polystyrene microparticles (3 μm) (Polysciences) were incubated with ICAM-1/human Fc chimera (R&D Systems). Beads were added to thymocytes on glass slides that were precoated with poly-L-lysine. Cells were imaged with a Leica DMI 6000 B inverted wide-field microscope. Image data were processed with Leica Application Suite software. Raw data of cell tracks (acquired with the manual tracking plug-in from ImageJ) were used to determine mean speed, displacement, and arrest coefficients.

Two-photon microscopy of explanted thymic lobes

Two-photon imaging was performed as described (1) with some changes. For the generation of partial mixed bone marrow chimeras, C57BL/6 mice were sublethally irradiated at 800 rad and injected with 2×10^6 mixed bone marrow cells from nontransgenic wild type C57BL/6 mice (90%), and GFP- and RFP-expressing wild type or *αPix*$^{-}$ C57BL/6 mice (5% each). The thymic ventral lobes from mixed bone marrow chimeras were held in place by a washer strung with filaments in a dish and placed in a 37°C incubator on a Zeiss LSM710 microscopic stage equipped with a MaiTai DeepSee laser (Spectra-Physics, Mountain View, CA) tuned to 850–900 nm and a 20× NA 1.0 water dipping lens. GFP^{+}, RFP^{+} cells, and second harmonic generation signals of the capsule were detected using non-descanned detectors and Zeiss Zen software. Images of a 600 × 600 μm cortical area ~70 μm below the capsule were acquired every 20 s. Cells that were visible for a minimum of 3 min were tracked in *x* and *y* dimensions and analyzed as described above.

Protein analysis

The Rac-GTP pull-down was performed essentially as described with some modifications (23). Thymocytes were resuspended in PBS plus 0.1% BSA, washed once, and lysed with RIPA buffer. One tenth of each sample was used as a loading control. GTP-bound Rac was precipitated from cell lysates using PAK-CRIB-GST as bait and analyzed by immunoblot. βPIX was analyzed by immunoblot of thymocyte lysates using anti-βPIX (BD Biosciences) and anti-Lsc Ab (24).

Apoptosis assay

Thymocytes in RPMI 1640 medium (Life Technologies) plus 10% FBS, penicillin–streptomycin solution, nonessential amino acids (1×) (PAA Laboratories, Pasching, Austria), 1 mM NaPyruvate (PAA) and 100 μM β-mercaptoethanol (Life Technologies) were plated at 2×10^5 cells in wells coated with 5 μg/ml anti-CD3 where indicated, with or without 1 μg/ml soluble anti-CD28. Cells were harvested after 24 h, washed, and stained for surface markers. Samples were stained with 7-aminoactinomycin D (7-AAD) and Annexin V FITC (BD Biosciences). Alternatively, cells were stained for intracellular activated caspase-3 and analyzed by flow cytometry.

TCR signaling

For detection of activated ERK, cells were stained for lineage markers together with hamster anti-CD3 Ab (2C11). After serum starvation for 20 min, cells were stimulated by TCR-crosslinking with goat $F(ab')_2$ anti-hamster IgG (STAR104; AbD Serotec), fixed with paraformaldehyde, permeabilized with methanol, stained with anti–phospho-ERK and analyzed by FACS.

For ratiometric measurement of calcium, cells were stained with Fluo3 and Fura Red (Life Technologies), followed by anti-CD4, anti-CD8, and 15 μg/ml anti-CD3 (2C11), and analyzed by FACS. A baseline level was recorded for 30 s prior to the induction of calcium influx by cross-linking CD3 with 6.5 μg/ml anti-hamster. Maximal influx was stimulated with 2 μM ionomycin.

Flow cytometry

Cells were labeled with Abs listed in Supplemental Table I and analyzed using a BD FACSCanto II flow cytometer, BD FACSDiva software, and FlowJo (Tree Star). For intracellular protein detection, cells stained for surface markers were fixed with 4% paraformaldehyde, permeabilized with BD Perm/Wash solution (BD Biosciences), and incubated with the indicated Abs against intracellular proteins. For conjugate formation of thymocytes and B cells, CD43^{-} B cells were purified on an autoMACS Pro (Miltenyi Biotec), and pulsed overnight with 10 μg/ml OVA peptide (JPT Peptide Technologies) in the presence of 30 μg/ml LPS (Sigma-Aldrich). B cells were mixed at a 1:1 ratio with OT-II^{+} thymocytes and analyzed for conjugate formation by FACS of CD8^{+} B220^{+} cell doublets (>95% of CD8^{+} cells in the thymus are DP thymocytes) as described (12). For transwell migration assays, 5-μm–pore membranes (Corning Costar) were coated with 3 μg/ml recombinant mouse ICAM-1/human Fc chimera (R&D Systems) plus anti-CD3 (2C11) where indicated and blocked with 2% BSA. Migration of cells to CXCL12 (200 ng/ml) or CCL25 (100 ng/ml) was analyzed as described (12).

Thymic section imaging

Freshly prepared thymi were embedded in Tissue Freezing Medium (Leica Microsystems) and snap frozen in methyl butane at −50°C. For immunofluorescence microscopy, 18-μm-thick sections were stained with anti–CD8-PE and anti–CD4-APC Abs.

In vivo BrdU incorporation assay

Mice were injected i.p. with 20 mg/ml BrdU and fed drinking water containing BrdU (1 mg/ml) with 2% glucose for 2 d. BrdU incorporation in thymocytes stained for CD4 and CD8 was analyzed by FACS with the BrdU Flow Kit (APC or FITC; BD Biosciences).

Results

Increased migration of αPix- thymocytes on 2D surfaces

In transwell migration assays, *αPix*$^{-}$ T and B cells show increased chemokinesis and increased chemotaxis (12). To determine whether *αPix*$^{-}$ thymocytes also show increased migration in vitro, we measured the transwell migration of all thymocyte subsets (DN, DP, CD4^{+}SP, and CD8^{+}SP) to CXCL12 (also known as SDF-1) and CCL25 (also known as TECK). In all cases, including the wells without chemokines, *αPix*$^{-}$ thymocyte migration was greatly increased compared with wild type thymocytes (Fig. 1A). Receptors for CXCL12 (CXCR4) and CCL25 (CCR9) were expressed normally on *αPix*$^{-}$ thymocytes (Supplemental Fig. 1). Thus, αPIX restricts not only chemokine-induced migration, but also basal migration of thymocytes.

Lymphocytes use integrins to generate traction force in certain contexts, such as during transendothelial or 2D surface migration (25, 26). PIX and GIT proteins associate with many integrin-regulating proteins and are involved in integrin-dependent functions (10, 27). To determine whether the increased transwell migration of αPIX knockout thymocytes is also evident in an

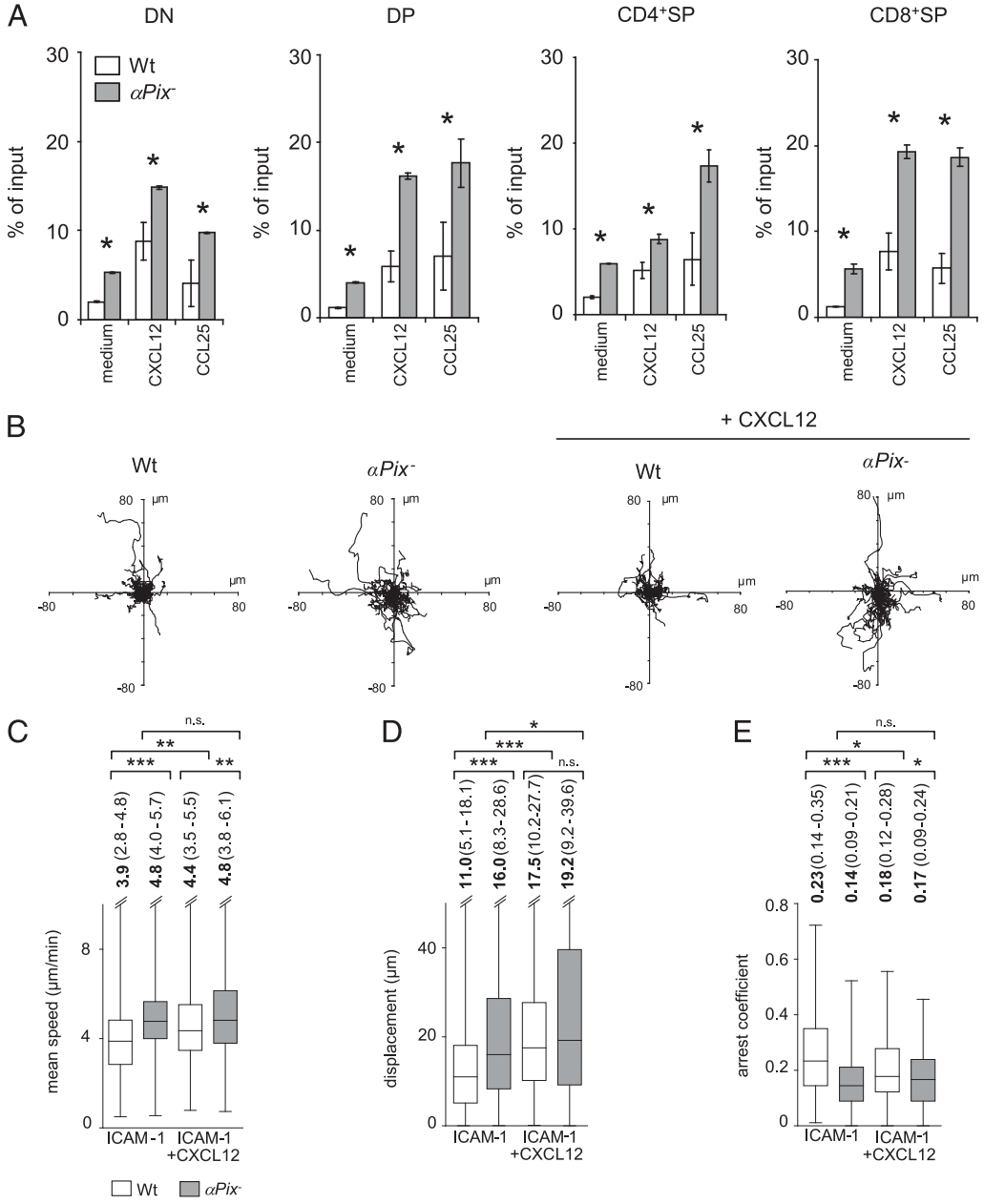

FIGURE 1. Increased motility of αPix^{-} thymocytes in vitro. (**A**) Transwell migration to CXCL12 or CCL25. Results expressed as the mean percentage ± SD of migrated cells to input cells, from one of three representative experiments. *$p < 0.05$ (Student t test). (**B**–**E**) Live cell imaging of thymocyte migration on 2D substrates. Wild type and αPix^{-} thymocytes stained with CFSE (green) or CMRA (red), respectively, were plated together on immobilized ICAM-1 and treated with soluble CXCL12 where indicated. Images were recorded at 10× magnification every 10 s for 30 min. (B) Cell tracks from one of four representative experiments, scaled to 80 μm. (C) Average speeds of all cells from four experiments (n = 355, 367, 341, and 256). (D) Average displacement from origin in 30 min combining four experiments, as in (C), and (E) arrest coefficients of thymocytes from two experiments (n = 100 each). Single-cell data are shown with the median ± interquartile range.*$p < 0.05$, **$p < 0.001$, ***$p < 0.0001$ (Mann–Whitney U test).

integrin-dependent context and corresponds to cellular velocity, we analyzed αPix^{-} thymocyte 2D motility on slides coated with immobilized ICAM-1 (LFA-1 ligand) in the presence or absence of CXCL12. An overlay of trajectories of individual thymocytes confirmed that αPix^{-} thymocytes were appreciably more motile than wild type thymocytes on surfaces coated with immobilized ICAM-1 (Fig. 1B). The effect was not related to altered expression of LFA-1 (CD11a/α_L chain), as this was normal (Supplemental Fig. 1). The aggregated mean speeds of single cells showed that αPix^{-} cells indeed migrate faster than wild type cells (Fig. 1C). Median displacement on ICAM-1 was also increased for αPix^{-} thymocytes, consistent with the observed velocity increases (Fig. 1D). Although wild type thymocyte velocity and displacement were enhanced by the addition of CXCL12, the αPix^{-} velocity levels were unaffected because they already exceeded the maximal levels attained by wild type on ICAM-1 plus CXCL12 (Fig. 1C, 1D). Because thymocyte displacement is punctuated by many stops and turns, we also analyzed the instantaneous velocities of single cells and determined arrest coefficients. We found a substantial reduction of arrest intervals for αPix^{-} thymocytes migrating on ICAM-1 without added CXCL12 (Fig. 1E). The addition of CXCL12 decreased the arrest coefficients of wild type thymocytes to levels similar to those of αPix^{-} thymocytes, but had no effect on αPix^{-} thymocytes (Fig. 1E). αPix^{-} thymocytes showed decreased arrest intervals along with increased migration speeds and displacement.

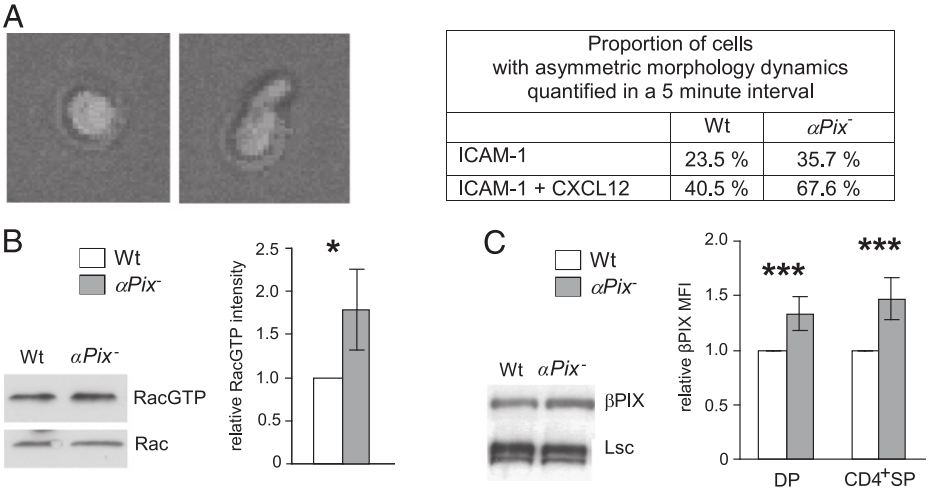

FIGURE 2. Increased cytoskeletal-related signaling in αPix^{-} thymocytes. (**A**) Abnormal morphology of αPix^{-} thymocytes. Thymocytes from wild type and αPix^{-} mice were plated on immobilized ICAM-1 alone or with added CXCL12 and recorded every 10 s by widefield, live cell imaging at 40× magnification for 5 min. Thymocytes were classed in two groups: cells that stayed mainly round during the 5-min observation period showing only small, broad protrusions (representative image, *left panel*) and cells that changed morphology extensively, showing irregular shapes and forming long protrusions (representative image, *right panel*). The table shows the percentages of the latter cell type in wild type and αPix^{-} thymocytes. (**B**) Increased Rac activation in αPix^{-} thymocytes. Rac-GTP was measured in freshly isolated thymocytes using a CRIB domain pull-down assay. Immunoblot analysis of RacGTP (*top panels*) and total Rac (*bottom panels*) in αPix^{-} thymocytes was quantified (*bar graph*) using densitometry and normalized to wild type levels. (**C**) Increased expression of βPIX in αPix^{-} thymocytes. Levels of βPIX and an unrelated RhoGEF, Lsc used as a loading control, were detected by immunoblot analysis (*left panel*). βPIX expression was also measured in αPix^{-} DP and $CD4^{+}SP$ thymocytes using flow cytometric analysis of thymocytes stained intracellularly for βPIX and normalized to expression of βPIX in wild type thymocytes ($n = 6$ each). $^{*}p < 0.05$ (Student t test), $^{***}p < 0.0001$ (Mann-Whitney U test).

Altered signaling to the cytoskeleton in αPix^{-} thymocytes

The morphology and dynamics of αPix^{-} cells in the 2D migration assays appeared qualitatively different from wild type cells. To quantify this finding, we counted cells that displayed dynamic and irregular or asymmetric borders versus cells that remained round on immobilized ICAM-1 (Fig. 2A). In both the presence and absence of CXCL12, a greater percentage of αPix^{-} thymocytes showed irregular borders and appeared to be in constant motion. These data suggest that αPix^{-} thymocytes have an intrinsic tendency to undergo increased shape flux, which can lead to increased migration on substrates that permit traction force. As the increased cytoskeletal dynamics could reflect abnormal activation of GTPases, we tested freshly isolated thymocytes for the presence of Rac-GTP and found that the basal level of Rac activation was indeed significantly higher in the absence of αPIX (Fig. 2B). This finding was unexpected because αPIX is a RhoGEF, and its loss should result in lower levels of Rac activation. We therefore tested whether expression of another RhoGEF, the αPIX homolog βPIX, was affected by the loss of αPIX, and found that it was increased ~50% in αPix^{-} thymocytes (Fig. 2C). Together, these data show that the absence of αPIX results in higher βPIX expression and basal Rac activation, which is consistent with an increase in cytoskeletal shape changes for αPix^{-} thymocytes.

Impaired positive selection in TCR-transgenic αPix^{-} mice

We previously reported that αPix^{-} mice on a mixed C57BL/6 and 129Sv background have normal numbers of thymocytes, including $CD4^{+}CD8^{+}$ DP thymocytes and $CD4^{+}$ or $CD8^{+}$ SP subsets, and reduced numbers of peripheral T cells (12). However, defects affecting thymocyte development are often masked by redundant homeostatic mechanisms to ensure sufficient numbers of thymocytes and T cells (1). We therefore introduced αβTCR transgenes into αPix^{-} thymocytes to limit the TCR repertoire of the thymocyte pool and to reveal any previously hidden developmental defects. Wild type and αPix^{-} mice were crossed to MHC class II–restricted TCR-transgenic mice that give rise to monoclonal $CD4^{+}$ SP thymocytes, OT-II and DO11.10, on the C57BL/6 and BALB/C backgrounds, respectively. Overall numbers of thymocytes in $DO11.10^{+}$ αPix^{-} and $OT\text{-}II^{+}$ αPix^{-} TCR-transgenic thymi were slightly increased (Fig. 3D, Supplemental Fig. 2C). However, $CD4^{+}SP$ thymocytes in αPix^{-} mice were ~3-fold reduced in $DO11.10^{+}$ mice and ~2-fold lower in $OT\text{-}II^{+}$ mice (Fig. 3A, 3D; Supplemental Fig. 2A, 2C), parallel with an increase in DP cells. Reductions in TCR^{hi} populations, identified with KJ1-26 mAb for DO11.10 and anti-Vα2 for OT-II, confirmed the reduction of the $CD4^{+}SP$ cell population (Fig. 3B, 3D; Supplemental Fig. 2B, 2C). The average percentage of $CD69^{+}KJ1\text{-}26^{hi}$ postselection thymocytes in the DP population was also significantly reduced in αPix^{-} mice, which is consistent with a defect in positive selection (Fig. 3E). Similarly, the numbers of $CD5^{hi}TCR^{hi}$ DP thymocytes were lower in $DO11.10^{+}$ αPix^{-} mice (Fig. 3E, Supplemental Fig. 2D). Moreover, upregulation of CD5, which correlates with intensity of TCR-mediated signaling during selection (28), was reduced on $DO11.10^{+}$ αPix^{-} DP but not $CD4^{+}SP$ thymocytes (Supplemental Fig. 2D). Images of thymic sections from $DO11.10^{+}$ αPix^{-} mice also showed considerable reductions in medullary areas and increased cortical areas compared with $DO11.10^{+}$ wild type mice, consistent with the decreased SP/DP ratio (Fig. 3C).

To determine whether the defective output of $CD4^{+}SP$ thymocytes was intrinsic to hematopoietic cells, wild type and αPix^{-} hosts were reconstituted with bone marrow stem cells from $DO11.10^{+}$ wild type or $DO11.10^{+}$ αPix^{-} mice (Fig. 3F). The generation of $KJ1\text{-}26^{hi}$ SP thymocytes from $DO11.10^{+}$ αPix^{-} bone marrow–to–wild type hosts was strongly reduced compared with wild type–to–wild type (average of 8.3% versus 23.2%), but chimeras using αPix^{-} mice as hosts and $DO11.10^{+}$ wild type mice as donors were essentially normal (average of 24.5% $KJ1\text{-}26^{hi}$; Fig. 3F, Supplemental Fig. 3A). Numbers of $CD69^{+}TCR^{hi}$ postselection DP thymocytes were also considerably reduced among $DO11.10^{+}$ αPix^{-}donor cells compared with $DO11.10^{+}$ wild type donor cells (Supplemental Fig. 3B). These reconstitution data showed that radiation-resistant cells in the αPix^{-} thymus are able to support proper thymocyte development and are consistent with a defect in positive selection.

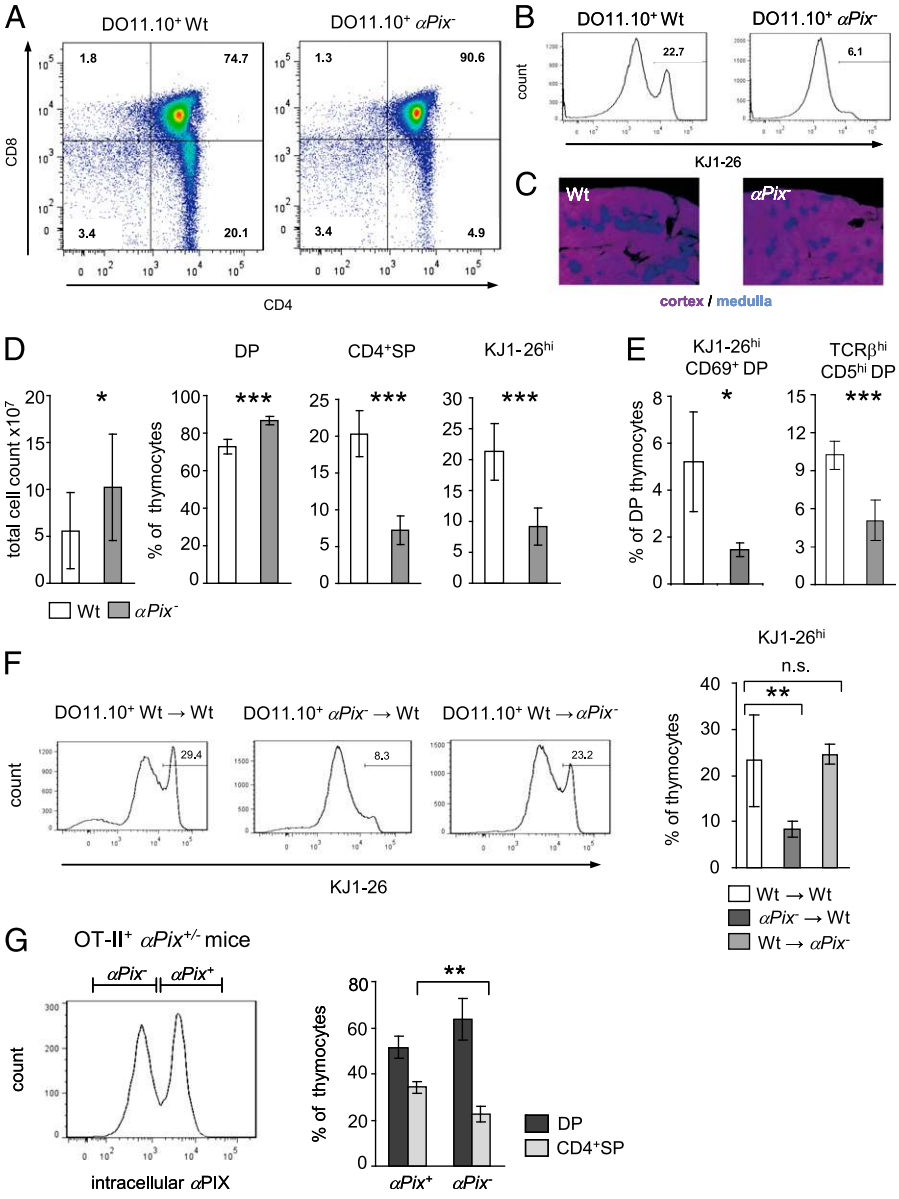

FIGURE 3. Reduced positive selection in TCR-transgenic αPix^{-} mice. Expression of CD4, CD8, and clonotypic TCR (KJ1-26) analyzed by flow cytometry shown as (**A**) dot plots and (**B**) single-color histograms of KJ1-26 expression. (**C**) Thymic slices stained with anti-CD4 (blue) and anti-CD8 (red) Abs. DP thymocytes appear purple and highlight cortical regions, whereas $CD4^{+}$ SP thymocytes (blue) are localized to medullary regions of the thymus. (**D**) Total numbers of thymocytes, relative numbers of $CD4^{+}CD8^{+}$ DP and $CD4^{+}$ or $CD8^{+}$ SP cells, and relative numbers of KJ1-26^{hi} total thymocytes from DO11.10^{+} wild type or DO11.10^{+} αPix^{-} mice ($n \geq 5$ each). (**E**) Average percentages of $CD69^{+}$ KJ1-26^{hi} and $CD5^{hi}$ TCR^{hi} post-selection DP thymocytes among DO11.10^{+} wild type or DO11.10^{+} αPix^{-} DP thymocytes. (**F**) Flow cytometric analysis of thymocytes from irradiated mice reconstituted with bone marrow cells from DO11.10^{+} wild type or DO11.10^{+} αPix^{-} mice with donors and recipients indicated on top of representative histograms of KJ1-26 expression on total thymocytes (*left panel*) and average percentage of KJ1-26^{hi} thymocytes from all experiments (*right panel*; $n \geq 3$). (**G**) Average percentages of DP and $CD4^{+}$SP thymocytes in αPix^{+} and αPix^{-} thymocytes from OT-II^{+} $\alpha Pix^{+/-}$ mice. Results are shown as mean ± SD. $^{*}p < 0.05$, $^{**}p < 0.001$, $^{***}p < 0.0001$ (Student *t* test).

Although wild type thymocytes developed normally in the wild type and αPix^{-} hosts (Fig. 3F), the macrophages and DCs in these mice derive from the wild type bone marrow donor cells. In the αPix^{-}-to–wild type mice, the macrophages and DCs are also αPix^{-}, and it could be argued that the αPix^{-} defect is not intrinsic to the thymocytes. Therefore, we wanted to assess the development of αPix^{-} thymocytes in an environment that sustains normal development of wild type thymocytes. To do this, we took advantage of the fact that the αPix gene is located on the X chromosome. In female mice, one of the two X chromosomes is randomly inactivated, thus OT-II^{+} $\alpha Pix^{+/-}$ females have both αPix^{+} and αPix^{-} thymocytes, macrophages, and DCs in the same thymus. We observed a comparable decrease in αPix^{-} $CD4^{+}$SP and increase in αPix^{-} DP thymocytes in OT-II^{+} $\alpha Pix^{+/-}$ females (Fig. 3G, Supplemental Fig. 3C), as in the transgenic αPix^{-} mice. Together, these data show that TCR-transgenic αPix^{-} thymocytes have a cell-intrinsic developmental disadvantage at the DP-to-$CD4^{+}$SP transition.

Normal negative selection in αPix^{-} mice

To measure thymocyte output in the absence of αPIX, we treated mice with a prolonged dose of BrdU and quantified $BrdU^{+}$ thymocytes. Numbers of $BrdU^{+}$ DP thymocytes were normal in DO11.10^{+} αPix^{-} mice, but $BrdU^{+}$ $CD4^{+}$SP thymocytes were significantly reduced, indicating that the reduction of $CD4^{+}$SP thymocytes results from a decreased output from the DP pool of thymocytes (Fig. 4A). We next examined cell death in ex vivo and cultured thymocytes by measuring activated caspase-3^{+} apoptotic cells and Annexin V^{+}/7-AAD^{+} dead cells. We found no differences in numbers of wild type and αPix^{-} thymocytes that were cultured for 24 h, either with or without TCR stimulation to induce apoptosis, indicating that signaling from TCR to apoptosis is not impaired by the lack of αPIX (Fig. 4B). The reduction in positively selected thymocytes in αPix^{-} mice implied that there should be increased loss of thymocytes due to death by neglect. However, we tested freshly isolated ex vivo thymocytes and observed a significant increase only in apoptotic cells, but not in dead cells from αPix^{-} TCR-transgenic mice (Fig. 4B), possibly because thymocytes that fail positive selection are rapidly consumed by thymic macrophages and we can detect only the thymocytes that are in earlier stages of apoptosis.

Negative selection of thymocytes was tested using the MHC class I–restricted H-Y TCR-transgenic system to induce negative

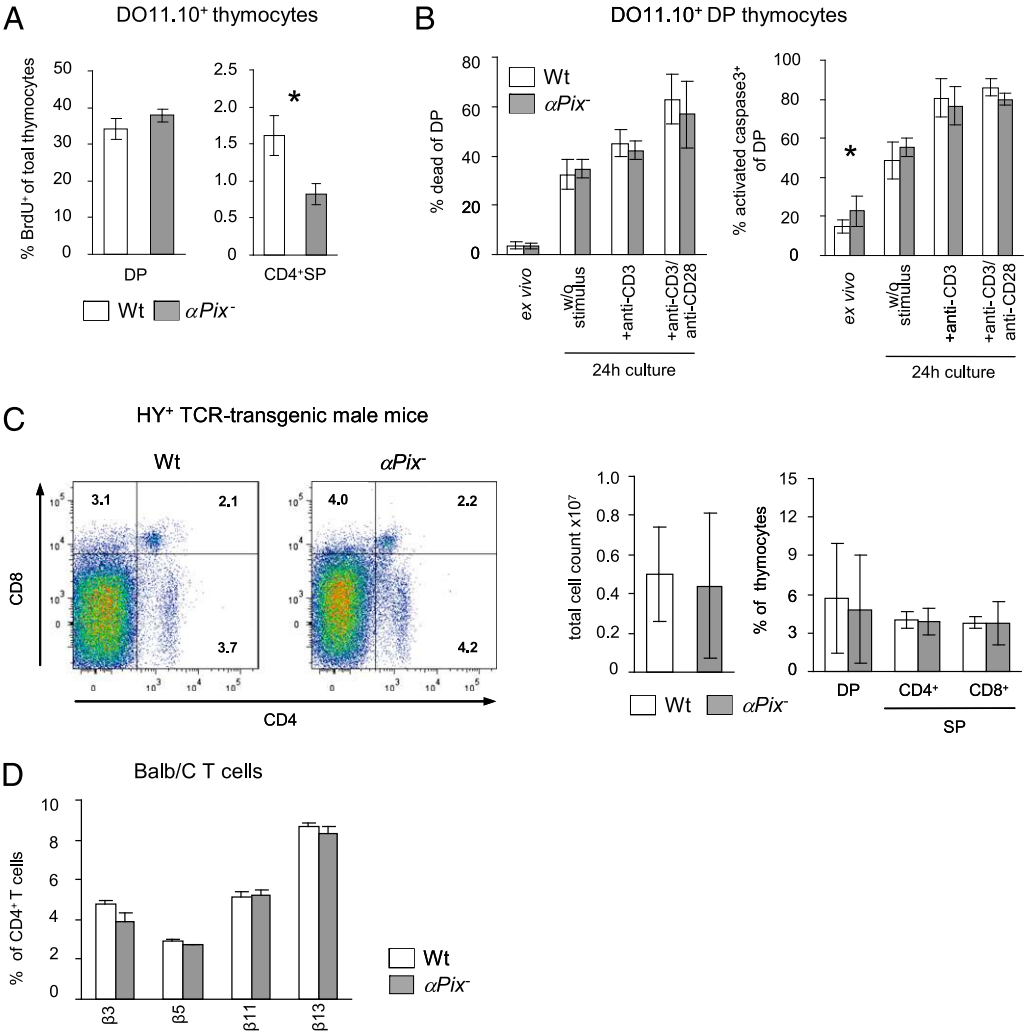

FIGURE 4. Normal negative selection in TCR-transgenic αPix^- mice. (**A**) BrdU$^+$ DP or CD4$^+$SP cells from DO11.10$^+$ wild type and DO11.10$^+$ αPix^- mice after 48 h of sustained BrdU treatment, percentages averaged from three mice. (**B**) Ex vivo and TCR-induced apoptosis of DO11.10$^+$ wild type and DO11.10$^+$ αPix^- thymocytes immediately after isolation or following 24 h of culture with immobilized anti-CD3 and costimulatory anti-CD28 Abs as indicated. Cell death or apoptosis was assessed by Annexin V binding and 7-AAD incorporation or by intracellular detection of activated caspase 3. Percentages of dead (AnnexinV$^+$ 7/AAD$^+$) or apoptotic (activated caspase-3$^+$) DP thymocytes ($n \geq 3$). (**C**) Negative selection in H-Y$^+$ TCR-transgenic wild type and αPix$^-$ male mice analyzed by flow cytometry. Representative CD4/CD8 dot plots and percentages of DP and CD4$^+$SP thymocytes averaged from three experiments. (**D**) Expression of negatively selected TCR β-chains in BALB/C mice. Splenic lymphocytes from TCR nontransgenic BALB/C mice stained for CD4, CD8, and TCR β-chains β3, β5, β11 (negatively selected) and β13 (positively selected) and frequency on CD4$^+$ T cells analyzed with FACS ($n = 2$ each). Results are shown as mean ± SD. *$p < 0.05$ (Student t test).

selection of thymocytes specific for the male H-Y Ag presented in male mice (18), but no impairment was observed in αPix^- mice (Fig. 4C). Additionally, expression of TCR β-chains (β3, β5, and β11) is low in BALB/C mice because of negative selection (29), but splenic T cells carrying these β-chains or the positively selected β13 chain were present at normal frequencies in αPix^- BALB/C mice, indicating that negative selection was operational (Fig. 4D). Together, these data indicate a defect in thymocyte positive selection in αPix^- TCR-transgenic mice.

Normal TCR signaling in αPix$^-$ thymocytes

We previously reported that TCR signaling to calcium fluxing and ERK activation were normal in αPix^- T cells (12). TCR signaling defects can affect positive selection. In particular, intracellular calcium levels regulate migration and arrest of thymocytes during positive selection (3). We therefore assessed TCR-induced calcium fluxing and ERK phosphorylation in DO11.10$^+$ αPix^- thymocytes. Both signaling pathways were activated normally in the absence of αPIX (Fig. 5A, 5B). TCR signaling is also required to activate pair formation between T cells and APCs bearing cognate pMHC. In peripheral T cells, αPIX is required for the formation of conjugates, but its role in thymocytes is unknown (12). We mixed wild type B cells pulsed with OVA peptide as APCs with DO11.10$^+$ wild type or DO11.10$^+$ αPix^- DP thymocytes and counted pairs formed, but observed no defects resulting from the loss of αPIX (Fig. 5C). In addition, we tested TCR induction of CD69 upregulation in OT-II$^+$ αPix^- thymocytes, but found no defects in TCR signaling to CD69 (Fig. 5D).

Increased motility of αPix$^-$ thymocytes during positive selection

The increased motility of the αPix^- thymocytes in vitro, coupled with the defects in αPix^- thymocyte development, led us to investigate αPix^- thymocyte migration in vivo in the thymic cortex. To compare wild type and αPix^- thymocyte migration in the thymus, we generated chimeric mice containing both GFP-labeled wild type thymocytes and RFP-labeled αPix^- thymocytes. Two-photon microscopy was used to image cortical regions in intact,

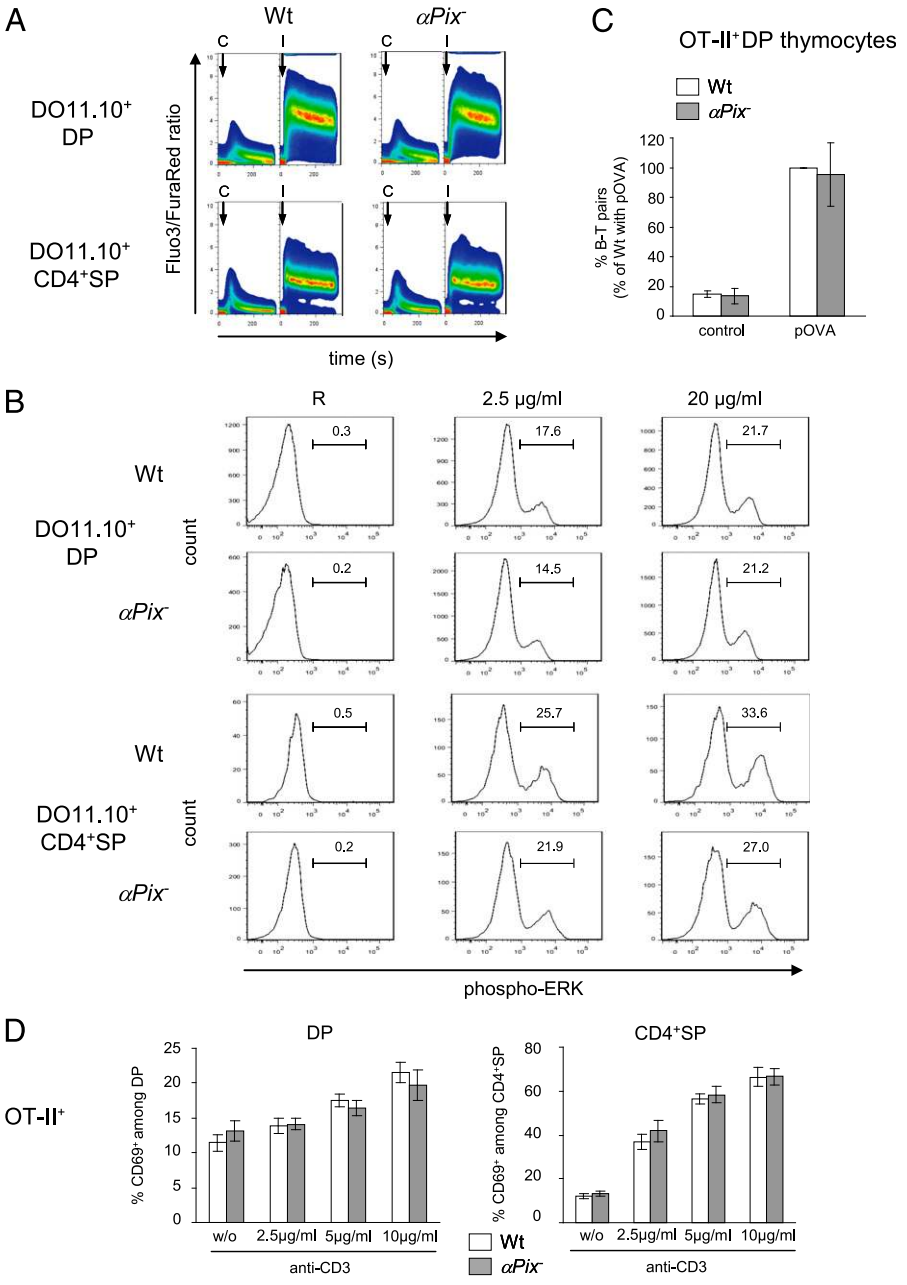

FIGURE 5. TCR signaling in αPix^{-} thymocytes. (**A**) TCR activation of calcium influx in DO11.10^{+} wild type and DO11.10^{+} αPix^{-} thymocytes measured by ratiometric FACS. CD3-crosslinker ("C") or ionomycin ("I") indicated by arrows. (**B**) TCR activation of ERK phosphorylation measured intracellularly by FACS shown as a representative histogram (n = 3). (**C**) Conjugate formation between OT-II^{+} wild type or OT-II^{+} αPix^{-} thymocytes and OVA-peptide–pulsed B cells. Average percentages from three independent experiments normalized to wild type conjugates in the presence of OVA-peptide. (**D**) TCR activation of CD69 upregulation in OT-II^{+} wild type or OT-II^{+} αPix^{-} thymocytes cultured for 24 h on varying doses of immobilized anti-CD3. Results are averaged from three independent experiments.

transplanted thymic lobes (Fig. 6A). Because RFP and GFP transgenes are expressed at much lower levels in immature DP than in mature SP cells, we amplified signals to increase detection, which had the side effect of enhancing autofluorescent signals (yellow) of larger cells that were probably resident dendritic cells or macrophages. However, these cells were easily distinguishable from thymocytes because they were stationary, whereas the thymocytes moved continuously with no significant decline of motility during imaging (Supplemental Video 1). It was immediately apparent that αPix^{-} thymocytes were more motile, appearing and disappearing in the plane of focus with higher frequency and covering larger distances within the same time period than wild type thymocytes did (Fig. 6B, Supplemental Videos 1–4). An overlay plot of cell trajectories of cells tracked for 10 min confirmed the increased migration of αPix^{-} thymocytes in vivo (Fig. 6C). The mean displacement of αPix^{-} thymocytes was larger than that of wild type thymocytes at every time point measured (Fig. 6D). A direct correlation on a plot of displacement against the square root of time indicates a random walk path, typical for cortical thymocytes, and this was comparable for wild type and αPix^{-} thymocytes (Fig. 6D).

αPix^{-} cortical thymocytes migrated significantly faster than wild type thymocytes did, with a median speed of 6.3 μm/min (interquartile range, 5.3–7.7 μm/min) versus 4.8 μm/min for wild type (interquartile range, 4.1−5.5 μm/min), confirming the increased migration speed in vitro (Fig. 6E). Reversing the genetic GFP and RFP markers for wild type and αPix^{-} thymocytes did not change the results of the analysis (data not shown). Thymocytes migrate in a stop-and-go mode; therefore, we tested the duration of stopping in αPix^{-} thymocytes. We found that wild type thymocytes paused for a median 17% of the time (instantaneous velocity < 2 μm/min), but αPix^{-} thymocytes paused for only a median 10% of the time (Fig. 6E). Measurement of arrest intervals showed that αPix^{-} thymocytes were more than twice as likely to not stop at all during the 5-min observation interval (Fig. 6F). In addition, most long stops (≥40 s) were made by wild type thymocytes (Fig. 6F). Imaging of the intact thymus confirmed

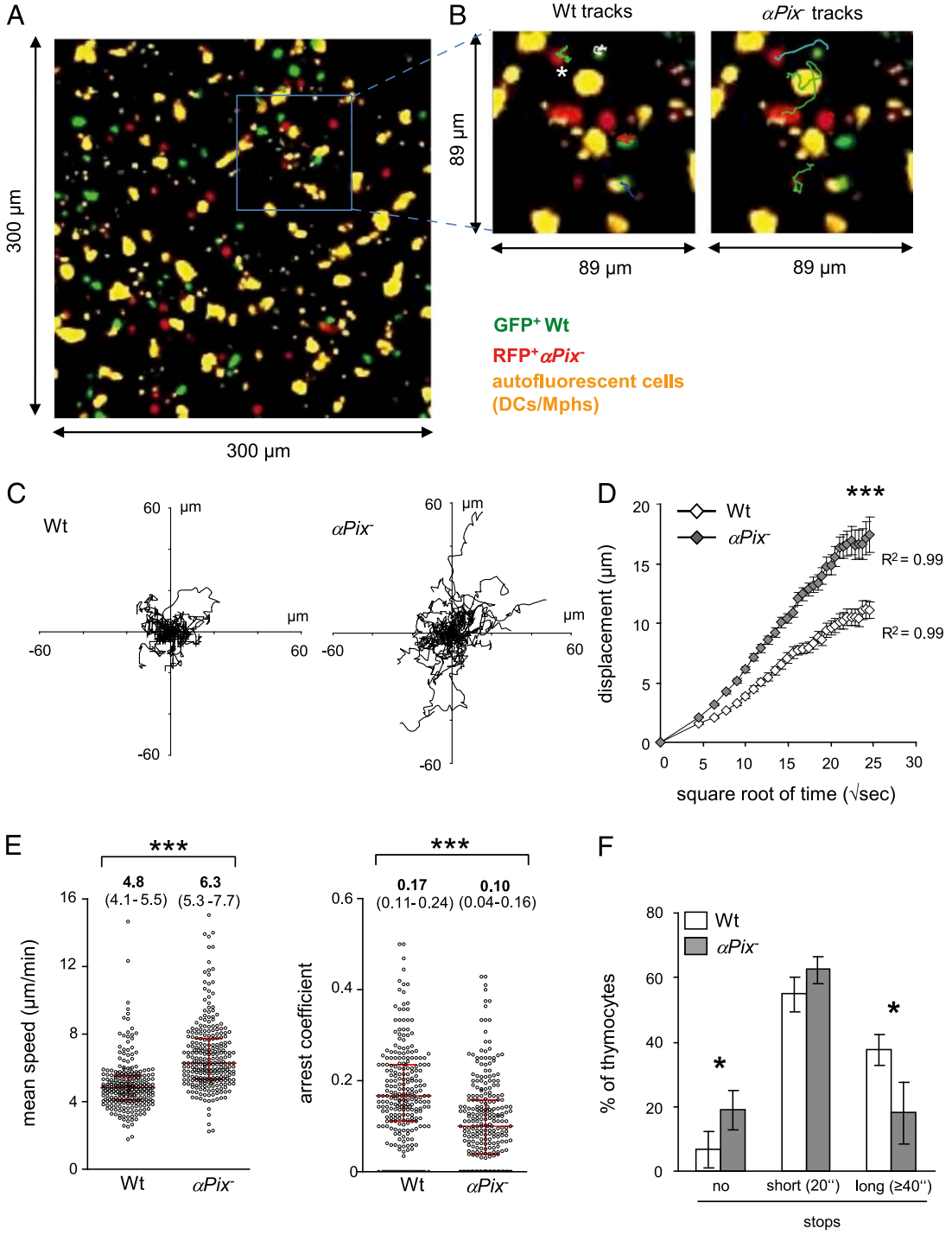

FIGURE 6. Increased motility of αPIX^{-} thymocytes in thymus. (**A**) Two-photon image of a cortical area ~70 µm below the dorsal capsule of a thymus from a GFP^{+} wild type (green) and RFP^{+} αPix^{-} (red) chimeric mouse. Larger, stationary autofluorescent cells are yellow (overlay of green and red autofluorescence) (Supplemental Video 1). (**B**) Migration tracks of wild type and αPix^{-} thymocytes shown in separate, duplicate images of a selected region from the larger frame shown in (A) (Supplemental Videos 2–4). Cell tracks are indicated with arbitrary colors. An asterisk indicates a wild type cell that moved out of focus. (**C**) Representative cell tracks during 10 min ($n = 40$ each), and (**D**) random walk motility shown by mean displacement ± SEM versus square root of time during 10 min (30 frames per cell), combining results of 251 wild type and 264 αPix^{-} thymocytes from a total five movies of three thymi analyzed in three independent experiments (R^2 = linear correlation coefficient). Significant differences determined at 10 min (corresponding to the square root of 600 seconds, 24.49 $sec^{1/2}$). ***$p < 0.0001$, Student t test. (**E**) Mean speeds (*left panel*) and arrest coefficients (*right panel*) of cells summarized from three independent experiments as in (D). ***$p < 0.0001$, Mann–Whitney U test. (**F**) Percentages of cells arresting for the indicated time periods (in seconds; instantaneous velocity < 2 µm/min) in a 5-min interval, combining three independent experiments, mean ± SD. *$p < 0.05$, Student t test).

the in vitro data that αPIX is necessary for restraining thymocyte migration speed and for promoting prolonged rest periods by thymocytes in the cortex. These data also suggest that the reduced stopping ability of αPix^{-} DP thymocytes likely decreases the chance of productive interactions with cortical APCs delivering positively selecting signals.

Reduced response to stop signals by hypermotile αPix⁻ thymocytes

To investigate *αPix*⁻ thymocyte arrest further, we used ICAM-1–coated beads as a model for cells that contact thymocytes in the cortex. Wild type thymocytes scanned the surface of the beads extensively for long periods without detaching (Fig. 7A, Supplemental Video 5). Almost all wild type thymocytes (~95%) stayed in contact with the beads for more than 200 s, but only ~60% of the *αPix*⁻ thymocytes interacted for more than 200 s with the beads (Fig. 7A, 7B; Supplemental Videos 5–6). Instead, almost half of the *αPix*⁻ thymocyte-bead interactions were less than 200 s. The majority of wild type thymocytes-bead interactions lasted as long as 25 min (1500 s), whereas only a small fraction of *αPix*⁻ thymocytes were capable of such long-lasting interactions (Fig. 7B).

Next, we assessed *αPix*⁻ thymocyte arrest on a physiologic substrate using a layer of OP9-DL1 stromal cells that can support positive selection (22). Most wild type thymocytes attached to the OP9-DL1 cells via small focal contacts and appeared to swing slowly around the contact point. In contrast, *αPix*⁻ thymocytes tended to wrench wildly at the attachment site (Fig. 7C, *I*; Supplemental Video 7). Wild type thymocytes were motile, but only a limited number of cells showed a pronounced migratory morphology or crawled for appreciable distances. In contrast, *αPix*⁻ thymocytes moved relatively far away or moved the length of several cell diameters before re-adhering (Fig. 7C, 7D, *II-IV*; Supplemental Videos 8–10). We also observed similar morphologic differences between wild type and *αPix*⁻ on the OP9-DL1 cells as described in Fig. 2, with a greater proportion of *αPix*⁻ cells appearing angular with long projections or multiple protrusions, or both, shown in a representative time-lapse series of images in Fig. 7D (*IV*; Supplemental Video 10). *αPix*⁻ thymocytes were clearly more motile than wild type thymocytes were on the cell layer, with *αPix*⁻ thymocytes displaying longer migration

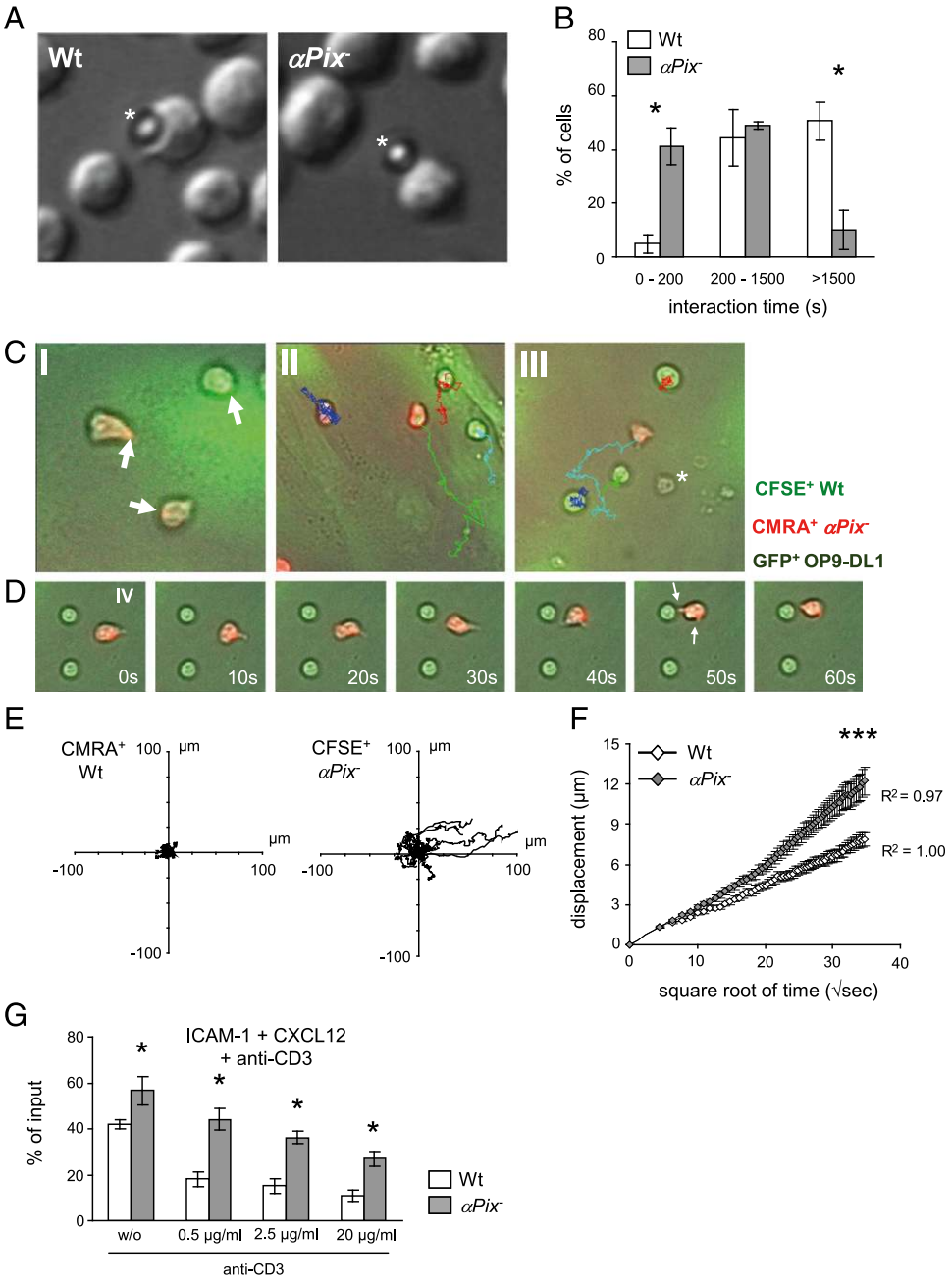

FIGURE 7. Decreased inhibition of *αPix*⁻ thymocyte migration. (**A** and **B**) Reduced contact time between *αPix*⁻ thymocytes and ICAM-1–coated beads (marked by asterisks) shown as (A) still images (from Supplemental Videos 5–6) and (B) as percentages of cells making contact with beads for the indicated time periods (in seconds). (**C–F**) Altered motility and morphology of *αPix*⁻ thymocytes (CMRA, red) plated together with wild type thymocytes (CFSE, green) on an OP9-DL1 cell monolayer (GFP⁺, green), original magnification ×40. (C) Representative snapshots (*I–III*) with cell tracks (arbitrary colors; Supplemental Videos 7–9). Arrows in *I* show tight contacts of *αPix*⁻ thymocytes with OP9-DL1 cells (dead cell in *III* marked with an asterisk). (D) A representative image sequence of *αPix*⁻ thymocytes at 10-s intervals from Supplemental Video 10. Arrows indicate prominent protrusions of the *αPix*⁻ thymocyte. (E) Cell tracks of wild type ($n = 24$) and *αPix*⁻ ($n = 33$) thymocytes on OP9-DL1 cells. (F) Mean displacement versus square root of time ± SEM, combining three experiments. (**G**) *αPix*⁻ thymocytes resist TCR-induced stop signals. Migration to CXCL12 through transwell membranes coated with ICAM-1 and increasing concentrations of anti-CD3. Mean ± SD from triplicates of one experiment representative of three. *$p < 0.05$, ***$p < 0.0001$, Student *t* test.

tracks (Fig. 7E) and increased average displacement (Fig. 7F). These data show that stable contact formation between thymocytes and stromal cells is greatly impaired in the absence of αPIX.

To determine the arrest response of αPix^{-} thymocytes to TCR stimulation, we tested transwell migration to CXCL12 by DP thymocytes through membranes coated with ICAM-1 and increasing concentrations of anti-CD3 Ab to trigger a TCR-induced stop signal (Fig. 7G). The addition of anti-CD3 did cause reduced migration of wild type and αPix^{-} thymocytes in a dose-dependent manner. However, the lowest dose of anti-CD3 blocked greater than 50% of wild type thymocytes from migrating, whereas the majority of αPix^{-} cells could still get through. Even at the highest dose of anti-CD3 used, αPix^{-} thymocytes were not restrained as fully as wild type, suggesting that the αPix^{-} cell-intrinsic increase in motility can overcome the TCR stop signal.

Discussion

Our study showed that αPIX is an inhibitor of thymocyte migration speeds and is necessary for complete thymocyte arrest on ICAM-1 and stromal cells. We observed a striking alteration in the morphology of migrating αPix^{-} thymocytes, suggestive of defects in control of actin dynamics. Although TCR-transgenic thymocytes from αPix^{-} mice had defective positive selection, negative selection appeared normal. TCR signaling, an important component of thymocyte maturation, was normal. Thus, the findings presented in this study are consistent with a role for αPIX in restraining thymocyte migration so as to enable pausing on cTECs, two key components of scanning behavior, to collect pMHC signals and become positively selected.

To our knowledge, the deletion of αPIX that we describe in this study is the only mutation to date that results in higher thymocyte migration speeds in the thymus linked to compromised development. PIX proteins have been implicated in signal transduction downstream of many receptors, including G protein-coupled receptors (GPCRs), integrins, and Ag receptors. We studied the migration of αPix^{-} thymocytes to receptors from each of these classes: chemokine receptor GPCRs, LFA-1 integrin, and TCR. In wild type thymocytes, GPCRs and integrin ligands enhance migration, and TCR induces migration arrest. In the absence of αPIX, signaling from these receptors to migration was still functional, but the baseline rate of migration was higher in every case. Thus, chemokines and integrin ligands promoted greater migration αPix^{-} thymocytes, and TCR activation caused less arrest of αPix^{-} thymocytes.

We found that the deletion of αPIX results in higher expression of βPIX. As PIX proteins and GIT proteins are constitutively bound together in an oligomeric complex, it is likely that βPIX can replace αPIX in the PIX-GIT complex. Thus, a similar replacement can happen upon the loss of GIT2, resulting in formation of a PIX-GIT complex with altered amounts of GIT1. This hypothesis could explain why $Git2^{-/-}$ and αPix^{-} mice have different migration phenotypes in vivo. We observed that αPix^{-} thymocytes migrate faster than wild type thymocytes in thymic cortex. In contrast, $Git2^{-/-}$ thymocytes have slower overall motility in vivo at areas with a high concentration of CXCL12 (6). The main interactions for GIT proteins are with Arf GTPases and paxillin, a key integrin-binding adaptor, and the main interactions for PIX proteins are with PAK, Rac1, and Cdc42. PIX and GIT proteins are also associated with many different additional proteins (10, 11, 30) that probably confer specificity on the PIX-GIT complex at different receptors or in different cell types. For example, GIT proteins downregulate GPCRs; therefore, chemokine signaling may be higher when GIT2 is missing than when αPIX is missing. It is also possible that these specific GIT2-dependent pathways are not apparent in an in vitro chemotaxis assay, in which only one or two specific activators or substrates are tested. Therefore, the differences in the αPIX and GIT2 phenotypes may reflect the different compositions of a βPIX-dominant complex or of a GIT1-dominant complex.

Although the reduction of thymocytes in transgenic TCR αPix^{-} mice could have been due to increased negative selection, we found no defects in PIX-mediated negative selection in the H-Y system, which causes apoptosis of H-Y–reactive thymocytes in the cortex (31), or in superantigen-induced deletion of TCR β-chains in BALB/C mice, which occurs in the medulla (32). Surprisingly, the impaired scanning behavior of αPix^{-} thymocytes did not compromise negative selection in the medulla or even in the cortex, where it might have been expected that the hypermotility of αPix^{-} thymocytes would result in less acquisition of signals, leading to both positive and negative selection. One possible explanation for this could be that the requirements for scanning and pMHC contacts are less stringent for negative selection than for positive selection. Negative selection in the medulla requires regulation of thymocyte migration patterns (7, 33), and thymocytes spend about twice as much time undergoing negative selection (4–5 d) than positive selection in the cortex (2–3 d) (34). If the increased migration of αPix^{-} thymocytes results in inefficient, error-prone scanning for pMHC, then the extra time thymocytes spend in the medulla can compensate for their poor performance. In addition, self-peptides in the medulla induce repeated encounters between thymocytes and mTECs and DCs in confined areas (33), which might ensure that αPix^{-} thymocytes would eventually encounter any autoactivating peptides. The normal negative selection we observed in the αPix^{-} thymus was supported by a lack of evidence of autoimmune disease in these mice, in contrast to CCR7 knockout mice that exhibit extensive autoimmune pathologies (35). Thymocytes from CCR7 knockout mice are unable to migrate to the medulla to undergo negative selection, but the αPix^{-} thymocyte hypermotile migratory response to chemokines probably ensures that any αPix^{-} $CD4^{+}SP$ thymocytes produced will succeed in responding to CCL19/21 and crossing the corticomedullary border, preventing the escape of autoimmune thymocytes to the periphery. Supporting the argument that αPIX may be more important for positive rather than negative selection, expression of αPIX mRNA in thymocyte subsets peaks in DP thymocytes undergoing positive selection and declines to lower levels in the postselection and mature SP thymocytes (http://www.immgen.org) (36).

αPIX expression is relatively high in immune cells compared with its homolog, βPIX, whereas βPIX is more broadly expressed in nonimmune tissues (12, 36). βPIX regulates formation of protrusions (14, 37–39), and overexpression of βPIX in fibroblasts and neurons alters the localization of βPIX itself, GIT1, Rac activity, and protrusions from a single leading edge to all around the cell periphery (37, 39). Moreover, increased Rac activity in fibroblasts and epithelial cells correlates with multiple peripheral lamellae, or protrusions, and increased random motility (40). We observed increased expression of βPIX and increased activation of Rac in αPix^{-} thymocytes, as well as increased protrusions and shape changes during their migration. Therefore, one possible model for the hypermotility phenotype of αPix^{-} thymocytes is that βPIX overcompensates for the loss of αPIX, leading to increased and delocalized Rac activity, driving formation of multiple protrusions all around the cell body and enhancing cell motility. Because immune cells use actin-based protrusions to generate traction force during locomotion (41), an increase in protrusions around the cell periphery would help to propel the thymocytes through the crowded environment of the thymus, similar to how a boat with increased numbers of rowers would

be faster than a similar boat with fewer rowers. To test this model, future studies will focus on mechanisms for PIX control of motility and thymocyte development in mice with mutations in both αPIX and βPIX.

Acknowledgments

We thank C. Schwarzer and H. Baumann for excellent technical assistance and Hans-Jörg Fehling for providing pTα-Cre and rosa26 tdRFP mice.

Disclosures

The authors have no financial conflicts of interest.

References

1. Ladi, E., X. Yin, T. Chtanova, and E. A. Robey. 2006. Thymic microenvironments for T cell differentiation and selection. *Nat. Immunol.* 7: 338–343.
2. Love, P. E., and A. Bhandoola. 2011. Signal integration and crosstalk during thymocyte migration and emigration. *Nat. Rev. Immunol.* 11: 469–477.
3. Bhakta, N. R., D. Y. Oh, and R. S. Lewis. 2005. Calcium oscillations regulate thymocyte motility during positive selection in the three-dimensional thymic environment. *Nat. Immunol.* 6: 143–151.
4. Bousso, P., N. R. Bhakta, R. S. Lewis, and E. Robey. 2002. Dynamics of thymocyte-stromal cell interactions visualized by two-photon microscopy. *Science* 296: 1876–1880.
5. Witt, C. M., S. Raychaudhuri, B. Schaefer, A. K. Chakraborty, and E. A. Robey. 2005. Directed migration of positively selected thymocytes visualized in real time. *PLoS Biol.* 3: e160.
6. Phee, H., I. Dzhagalov, M. Mollenauer, Y. Wang, D. J. Irvine, E. Robey, and A. Weiss. 2010. Regulation of thymocyte positive selection and motility by GIT2. *Nat. Immunol.* 11: 503–511.
7. Ueda, Y., K. Katagiri, T. Tomiyama, K. Yasuda, K. Habiro, T. Katakai, S. Ikehara, M. Matsumoto, and T. Kinashi. 2012. Mst1 regulates integrin-dependent thymocyte trafficking and antigen recognition in the thymus. *Nat. Commun.* 3: 1098.
8. Ehrlich, L. I., D. Y. Oh, I. L. Weissman, and R. S. Lewis. 2009. Differential contribution of chemotaxis and substrate restriction to segregation of immature and mature thymocytes. *Immunity* 31: 986–998.
9. Sanos, S. L., J. Nowak, M. Fallet, and M. Bajenoff. 2011. Stromal cell networks regulate thymocyte migration and dendritic cell behavior in the thymus. *J. Immunol.* 186: 2835–2841.
10. Frank, S. R., and S. H. Hansen. 2008. The PIX-GIT complex: a G protein signaling cassette in control of cell shape. *Semin. Cell Dev. Biol.* 19: 234–244.
11. Hoefen, R. J., and B. C. Berk. 2006. The multifunctional GIT family of proteins. *J. Cell Sci.* 119: 1469–1475.
12. Missy, K., B. Hu, K. Schilling, A. Harenberg, V. Sakk, K. Kuchenbecker, K. Kutsche, and K. D. Fischer. 2008. AlphaPIX Rho GTPase guanine nucleotide exchange factor regulates lymphocyte functions and antigen receptor signaling. *Mol. Cell. Biol.* 28: 3776–3789.
13. Castro-Castro, A., V. Ojeda, M. Barreira, V. Sauzeau, I. Navarro-Lérida, O. Muriel, J. R. Couceiro, F. X. Pimentel-Muíños, M. A. Del Pozo, and X. R. Bustelo. 2011. Coronin 1A promotes a cytoskeletal-based feedback loop that facilitates Rac1 translocation and activation. *EMBO J.* 30: 3913–3927.
14. Kuo, J. C., X. Han, C. T. Hsiao, J. R. Yates, III, and C. M. Waterman. 2011. Analysis of the myosin-II-responsive focal adhesion proteome reveals a role for β-Pix in negative regulation of focal adhesion maturation. *Nat. Cell Biol.* 13: 383–393.
15. Li, Z., M. Hannigan, Z. Mo, B. Liu, W. Lu, Y. Wu, A. V. Smrcka, G. Wu, L. Li, M. Liu, et al. 2003. Directional sensing requires G beta gamma-mediated PAK1 and PIX alpha-dependent activation of Cdc42. *Cell* 114: 215–227.
16. Hsieh, C. S., S. E. Macatonia, A. O'Garra, and K. M. Murphy. 1995. T cell genetic background determines default T helper phenotype development in vitro. *J. Exp. Med.* 181: 713–721.
17. Barnden, M. J., J. Allison, W. R. Heath, and F. R. Carbone. 1998. Defective TCR expression in transgenic mice constructed using cDNA-based alpha- and beta-chain genes under the control of heterologous regulatory elements. *Immunol. Cell Biol.* 76: 34–40.
18. Teh, H. S., H. Kishi, B. Scott, and H. Von Boehmer. 1989. Deletion of autospecific T cells in T cell receptor (TCR) transgenic mice spares cells with normal TCR levels and low levels of CD8 molecules. *J. Exp. Med.* 169: 795–806.
19. Hadjantonakis, A. K., and V. E. Papaioannou. 2004. Dynamic in vivo imaging and cell tracking using a histone fluorescent protein fusion in mice. *BMC Biotechnol.* 4: 33.
20. Luche, H., O. Weber, T. Nageswara Rao, C. Blum, and H. J. Fehling. 2007. Faithful activation of an extra-bright red fluorescent protein in "knock-in" Cre-reporter mice ideally suited for lineage tracing studies. *Eur. J. Immunol.* 37: 43–53.
21. Schmalzigaug, R., H. Phee, C. E. Davidson, A. Weiss, and R. T. Premont. 2007. Differential expression of the ARF GAP genes GIT1 and GIT2 in mouse tissues. *J. Histochem. Cytochem.* 55: 1039–1048.
22. Schmitt, T. M., R. F. de Pooter, M. A. Gronski, S. K. Cho, P. S. Ohashi, and J. C. Zúñiga-Pflücker. 2004. Induction of T cell development and establishment of T cell competence from embryonic stem cells differentiated in vitro. *Nat. Immunol.* 5: 410–417.
23. Harenberg, A., I. Girkontaite, K. Giehl, and K. D. Fischer. 2005. The Lsc RhoGEF mediates signaling from thromboxane A2 to actin polymerization and apoptosis in thymocytes. *Eur. J. Immunol.* 35: 1977–1986.
24. Girkontaite, I., K. Missy, V. Sakk, A. Harenberg, K. Tedford, T. Pötzel, K. Pfeffer, and K. D. Fischer. 2001. Lsc is required for marginal zone B cells, regulation of lymphocyte motility and immune responses. *Nat. Immunol.* 2: 855–862.
25. Alon, R., and Z. Shulman. 2011. Chemokine triggered integrin activation and actin remodeling events guiding lymphocyte migration across vascular barriers. *Exp. Cell Res.* 317: 632–641.
26. Lämmermann, T., and M. Sixt. 2009. Mechanical modes of 'amoeboid' cell migration. *Curr. Opin. Cell Biol.* 21: 636–644.
27. Rosenberger, G., and K. Kutsche. 2006. AlphaPIX and betaPIX and their role in focal adhesion formation. *Eur. J. Cell Biol.* 85: 265–274.
28. Azzam, H. S., J. B. DeJarnette, K. Huang, R. Emmons, C. S. Park, C. L. Sommers, D. El-Khoury, E. W. Shores, and P. E. Love. 2001. Fine tuning of TCR signaling by CD5. *J. Immunol.* 166: 5464–5472.
29. Simpson, E. 1993. T cell repertoire selection by mouse mammary tumour viruses. *Eur. J. Immunogenet.* 20: 137–149.
30. Mayhew, M. W., D. J. Webb, M. Kovalenko, L. Whitmore, J. W. Fox, and A. F. Horwitz. 2006. Identification of protein networks associated with the PAK1-betaPIX-GIT1-paxillin signaling complex by mass spectrometry. *J. Proteome Res.* 5: 2417–2423.
31. McCaughtry, T. M., T. A. Baldwin, M. S. Wilken, and K. A. Hogquist. 2008. Clonal deletion of thymocytes can occur in the cortex with no involvement of the medulla. *J. Exp. Med.* 205: 2575–2584.
32. Kappler, J. W., N. Roehm, and P. Marrack. 1987. T cell tolerance by clonal elimination in the thymus. *Cell* 49: 273–280.
33. Le Borgne, M., E. Ladi, I. Dzhagalov, P. Herzmark, Y. F. Liao, A. K. Chakraborty, and E. A. Robey. 2009. The impact of negative selection on thymocyte migration in the medulla. *Nat. Immunol.* 10: 823–830.
34. Klein, L. 2009. Dead man walking: how thymocytes scan the medulla. *Nat. Immunol.* 10: 809–811.
35. Kurobe, H., C. Liu, T. Ueno, F. Saito, I. Ohigashi, N. Seach, R. Arakaki, Y. Hayashi, T. Kitagawa, M. Lipp, et al. 2006. CCR7-dependent cortex-to-medulla migration of positively selected thymocytes is essential for establishing central tolerance. *Immunity* 24: 165–177.
36. Heng, T. S., M. W. Painter; Immunological Genome Project Consortium. 2008. The Immunological Genome Project: networks of gene expression in immune cells. *Nat. Immunol.* 9: 1091–1094.
37. Cau, J., and A. Hall. 2005. Cdc42 controls the polarity of the actin and microtubule cytoskeletons through two distinct signal transduction pathways. *J. Cell Sci.* 118: 2579–2587.
38. Za, L., C. Albertinazzi, S. Paris, M. Gagliani, C. Tacchetti, and I. de Curtis. 2006. betaPIX controls cell motility and neurite extension by regulating the distribution of GIT1. *J. Cell Sci.* 119: 2654–2666.
39. Zhang, H., D. J. Webb, H. Asmussen, and A. F. Horwitz. 2003. Synapse formation is regulated by the signaling adaptor GIT1. *J. Cell Biol.* 161: 131–142.
40. Pankov, R., Y. Endo, S. Even-Ram, M. Araki, K. Clark, E. Cukierman, K. Matsumoto, and K. M. Yamada. 2005. A Rac switch regulates random versus directionally persistent cell migration. *J. Cell Biol.* 170: 793–802.
41. Renkawitz, J., and M. Sixt. 2010. Mechanisms of force generation and force transmission during interstitial leukocyte migration. *EMBO Rep.* 11: 744–750.